ISSN 0021-3640, JETP Letters, 2021, Vol. 114, No. 2, pp. 92–97. © Pleiades Publishing, Inc., 2021.
Russian Text © The Author(s), 2021, published in Pis'ma v Zhurnal Eksperimental'noi i Teoreticheskoi Fiziki, 2021, Vol. 114, No. 2, pp. 89–95.

CONDENSED MATTER

Spin-Flop Transition in $Co_2B_2O_5$ Pyroborate

N. V. Kazak[a, *], N. A. Belskaya[a, b], E. M. Moshkina[a], L. A. Solovyov[c], E. V. Eremin[a, b, d], S. Yu. Gavrilkin[e], and S. G. Ovchinnikov[a, d]

[a] *Kirensky Institute of Physics, Federal Research Center KSC, Siberian Branch, Russian Academy of Sciences, Akademgorodok, Krasnoyarsk, 660036 Russia*

[b] *Reshetnev Siberian State University of Science and Technology, Krasnoyarsk, 660037 Russia*

[c] *Institute of Chemistry and Chemical Technology, Siberian Branch, Russian Academy of Sciences, Krasnoyarsk, 660036 Russia*

[d] *Siberian Federal University, Krasnoyarsk, 660041 Russia*

[e] *Lebedev Physical Institute, Russian Academy of Sciences, Moscow, 119991 Russia*

**e-mail: nat@iph.krasn.ru*

Received June 21, 2021; revised June 22, 2021; accepted June 22, 2021

Cobalt pyroborate $Co_2B_2O_5$ single crystals have been obtained by spontaneous crystallization from solution–melt. Powder X-ray diffraction measurements have revealed the triclinic symmetry $P\bar{1}$ with the lattice parameters $a = 3.1666(7)$ Å, $b = 6.1543(6)$ Å, $c = 9.2785(12)$ Å, $\alpha = 104.240(5)°$, $\beta = 90.841(14)°$, $\gamma = 92.064(16)°$, and $V = 175.10(5)$ Å^3. Magnetic properties have been studied in the temperature range of 4.2–300 K and in magnetic fields up to 90 kOe by measuring the static magnetization and molar heat capacity. A transition to an antiferromagnetic state has been detected at $T_N = 45$ K. A spin-flop transition occurs in the sample in strong magnetic fields.

DOI: 10.1134/S0021364021140058

INTRODUCTION

Transition metal borates and oxyborates have been actively studied recently as possible sources of Li- and Na-ion batteries [1–3]. The diversity of polyanion complexes formed from plane-triangle $(BO_3)^{3-}$ and/or tetrahedral $(BO_4)^{5-}$ groups makes it possible to obtain new materials with extraordinary magnetic, optical, magneto-optical, and magneto-electric properties. Borates with the structures of calcite $Me^{3+}BO_3$ [4–6], warwickite $Me^{2+}Me^{3+}BO_4$ [7–10], ludwigite $Me_2^{2+}Me^{3+}BO_5$ [11–14], and huntite $Me_4^{3+}(BO_3)_4$ [15–17], where Me^{2+} and Me^{3+} are 3*d* and 4*f* ions are the most studied. Magnetic transformations associated with the ordering of various spin subsystems, structural and electronic transitions accompanied by charge ordering, spin-reorientation transitions induced by strong magnetocrystalline anisotropy, and effects of frustrations of magnetic interactions in these materials have been actively studied for several decades.

At the same time, pyroborates with the general formula $Me_2^{2+}B_2O_5$ are much less studied. Divalent transition metal ions are responsible for magnetism in these materials. Pyroborates based on Mn [18, 19], Co [19], and Fe [20, 21] have been obtained and partially studied. It is established that homometallic pyroborates $Mn_2B_2O_5$, $Co_2B_2O_5$, and $Fe_2B_2O_5$ are low-temperature antiferromagnets with the Néel temperatures $T_N = 24$, 45, and 70 K, respectively. Pyroborates are crystallized in the triclinic symmetry $P\bar{1}$. Metal ions occupy two crystallographically nonequivalent positions M1 and M2 (2*i* positions according to Wyckoff) located in the center of oxygen octahedra (Fig. 1). The edge-sharing octahedra are joined in the M1–M2–M2–M1 row and propagate along a short crystallographic direction, forming ribbons. Ribbons are joined in a three-dimensional framework by $B1O_3$ and $B2O_3$ trigonal groups condensed in the $(B_2O_5)^{4-}$ polyanion complex.

The magnetic properties of manganese pyroborate are the most studied. The field dependence of the magnetization $M(H)$ of the $Mn_2B_2O_5$ demonstrates a cascade of spin reorientational transitions in the field range of 20–50 kOe. The low-field spin-flop transition at $H_{sf} = 25$ kOe was attributed to the reorientation of the magnetic moments of Mn^{2+} in the entire volume. The spin configuration of $Mn_2B_2O_5$ was proposed on the basis of the calculation of the electron density distribution with the maximum entropy method [22]. According to the proposed model, all coplanar ribbons in $Mn_2B_2O_5$ are ferromagnetic and

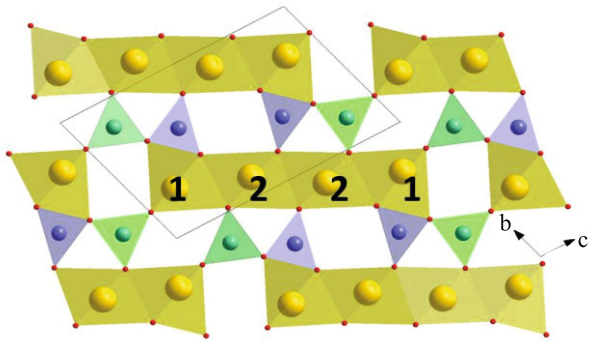

Fig. 1. (Color online) Crystal structure of the $Co_2B_2O_5$ pyroborate. The crystallographically nonequivalent positions of cobalt are marked by numbers. The green and blue triangles indicate nonequivalent boron positions B1 and B2, respectively.

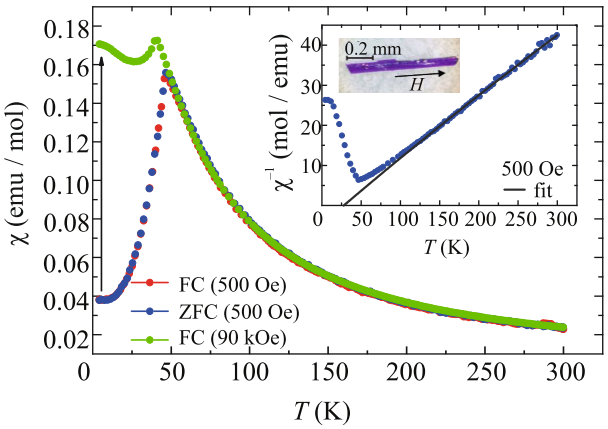

Fig. 2. (Color online) Temperature dependences of the magnetic susceptibility of the $Co_2B_2O_5$ single crystal measured in magnetic fields of 0.5 and 90 kOe. The arrow indicates an increase in the magnetic moment in a strong magnetic field. The inset shows (circles) the temperature dependence of the inverse magnetic susceptibility in a magnetic field of 0.5 kOe, (solid line) Curie–Weiss fit (1), and the photo of the $Co_2B_2O_5$ pyroborate single crystal; the direction of an external magnetic field is shown by an arrow.

the antiferromagnetic behavior is due to the antiparallel magnetic orientations between neighboring ribbons.

The present work is devoted to the study of cobalt pyroborate $Co_2B_2O_5$. The crystal structure was first studied in [23] and was then solved in detail in [24]. The effect of the magnetic ($Co^{2+} \rightarrow Mn^{2+}$) and nonmagnetic ($Co^{2+} \rightarrow Zn^{2+}$) substitutions on the crystal structure was studied in [25, 26], respectively. The partial substitution of manganese for cobalt ions leads to an increase in the lattice parameters and volume according to the ion radii $r(Co^{2+}) = 0.745$ Å and $r(Mn^{2+}) = 0.83$ Å [27]. To the best of our knowledge, the magnetic and electron properties of cobalt pyroborate were studied only in [19], where the magnetic susceptibility was measured in a field of 10 kOe. The effective magnetic moment determined from the fitting of the high-temperature part of the susceptibility is $4.96\mu_B$ per Co^{2+} ion. The optical absorption edge ~4.15 eV was determined from diffuse reflection spectra. The behavior of the magnetization of $Co_2B_2O_5$ in the magnetic field was not studied. Nevertheless, by analogy with manganese pyroborate, one can expect that $Co_2B_2O_5$ will demonstrate field-induced spin-reorientational transitions.

SYNTHESIS OF THE SAMPLES AND EXPERIMENTAL METHODS

$Co_2B_2O_5$ single crystals were obtained by the solution–melt method in the spontaneous crystallization regime from the initial components in the relation $Bi_2Mo_3O_{12} : 1.08Na_2B_4O_7 : 4.82CoO : 0.8B_2O_3$. The solution–melt was prepared by successive melting of initial oxides in a 100-cm^3 platinum crucible at a temperature of $T = 1100$°C. The prepared solution–melt was homogenized for 3 h at the temperature of $T = 1100$°C. After homogenization, the temperature in the oven was reduced first rapidly at a rate of $dT/dt = 100$°C/h to $T = 880$°C and then slowly at a rate of $dT/dt = 4$°C/day. The crucible was extracted from the oven after 48 h and the solution–melt was drawn. Single crystals were separated by etching in a 20% aqueous solution of nitric acid. The samples were pink–purple planar prisms elongated along the short crystallographic direction a with a parallelogram cross section and had dimensions of 0.01 × 0.5 × 1.0 mm.

The X-ray diffraction analysis was performed with a PANalyticalX'PertPRO powder diffractometer (CoK_α radiation, Netherlands) in the angular range of $2\theta = 5°–100°$. The refinement of the lattice parameters was performed from the total profile of the diffraction pattern using the derivative difference minimization method [28].

The static magnetization and heat capacity were measured in the temperature range of 4.2–300 K and in magnetic fields up to 90 kOe using a PPMS Quantum Design platform (Common Access Facility Centres of SB RAS and P.N. Lebedev Physical Institute of RAS). A single crystal with a mass of 0.43 mg was selected for magnetic measurements. The external magnetic field was applied parallel to the axis of the crystal (inset of Fig. 2). Measurements were performed in two regimes: cooling in an external magnetic field (FC) and zero-field cooling (ZFC). The heat capacity was measured on single-crystal samples with a total mass of 2 mg.

Table 1. Magnetic parameters of cobalt borates determined from the fitting of the high-temperature susceptibility

	$n_{Co^{2+}}$/f.u.	χ_0, emu/mol	C, emu K/mol	θ, K	μ_{eff}, μ_B/f.u.	μ_{eff}, μ_B/Co^{2+}
$Co_3BO_5^*$ [29]	2	$(1.3 \pm 0.3) \times 10^{-3}$	4.0 ± 0.1	11 ± 2	5.7 ± 0.1	4.0
$Co_{5/3}Nb_{1/3}BO_4$ [30]	1.67	$(1.6 \pm 0.2) \times 10^{-3}$	3.8 ± 0.1	-8.9 ± 2.4	5.5 ± 0.1	4.3
$Co_3B_2O_6$ [31]	3	$(1.8 \pm 0.9) \times 10^{-3}$	7.8 ± 0.5	-60.4 ± 8.3	7.9 ± 0.2	4.6
$Co_2B_2BO_5^{**}$	2	$(1.5 \pm 0.3) \times 10^{-3}$	6.0 ± 0.1	27.9 ± 1.6	6.9 ± 0.1	4.9

*It is assumed that Co^{3+} ions are in a low-spin state ($S = 0$) and do not contribute to the magnetic moment. **Present work.

RESULTS

X-ray diffraction measurements showed that the obtained samples are crystallized in the triclinic symmetry $P\bar{1}$. The lattice parameters $a = 3.1666(7)$ Å, $b = 6.1543(6)$ Å, $c = 9.2785(12)$ Å, $\alpha = 104.240(5)°$, $\beta = 90.841(14)°$, $\gamma = 92.064(16)°$, and $V = 175.10(5)$ Å^3 are in good agreement with the previously reported data [19, 23, 24].

Figure 2 shows the temperature dependences of the magnetic susceptibility $\chi(T) = M/H$ measured in magnetic fields of 0.5 and 90 kOe. It is seen that FC and ZFC curves are imposed on each other in the entire temperature range, demonstrating a pronounced maximum near $T_N = 46$ K. The found antiferromagnetic transition temperature is close to that reported in [19]. The magnetization decreases rapidly below the transition temperature, approaching a value observed at room temperature. Such a behavior is inherent in an antiferromagnet when the external field is directed along the antiferromagnetism axis ($\chi_\parallel$). The magnetic susceptibility $\chi_\parallel(4.2\ \text{K}) = 0.04$ emu/mol in the single crystal is half the magnetic susceptibility χ_{poly} found in a polycrystalline sample [19], which indicates the presence of magnetic anisotropy in the studied pyroborate. In a strong magnetic field of 90 kOe, the anomaly associated with the magnetic transition is still clearly seen but it is shifted to low temperatures about 40 K. When the temperature decreases below T_N, the susceptibility decreases slightly and, then below $T = 25$ K, increases slowly. This behavior of $\chi(T)$ reflects a strong nonlinear field dependence of the magnetic moment. Strong difference in the behavior of $\chi(T)$ curves in a magnetically ordered phase measured in strong and weak fields is typical of the antiferromagnet undergoing a spin-reorientational transition. Thus, the susceptibility in a magnetic field of 90 kOe is characteristic of the spin-flop phase ($\chi_\perp$).

Using an approach previously applied to analyze the magnetic susceptibility of cobalt oxyborates [29–31], we processed the temperature dependence of the magnetic susceptibility of $Co_2B_2O_5$ by the modified Curie–Weiss law

$$\chi(T) = \chi_0 + \frac{C}{T - \theta}, \quad (1)$$

where χ_0 is the temperature-independent term, C is the Curie–Weiss constant, and θ is the Curie–Weiss temperature. Approximation with the parameters summarized in Table 1 is satisfactory in the temperature range of 150–300 K. The magnetic moment $4.9\mu_B$ per Co^{2+} ion is characteristic of a high-spin state with a small orbital contribution and is in good agreement with experimental values for the Co^{2+} ion ($S = 3/2$) in the octahedral environment [29–34].

Signatures of the spin-flop transition are clearly seen in the magnetic field dependences of the magnetization (Fig. 3a). A linear contribution exists in fields below 30 kOe. Near $H_{sf} = 75$ kOe, the magnetization changes stepwise and, then above 80 kOe, increases more slowly. The observed magnetic behavior indicates the reorientation of magnetic moments of Co^{2+} ions and a spin-flop transition. This transition is manifested in the dependence of the derivative $\partial M/\partial H$ as an intense maximum at H_{sf} (Fig. 3b). Measurements with decreasing field did not reveal hysteresis in the entire field range. The spin-flop transition in $Co_2B_2O_5$ is more extended in field compared to the transition in $Mn_2B_2O_5$ and the spin reorientation process has not yet been completed in fields of about 90 kOe. As the temperature increases, the anomaly associated with the spin-flop transition is smeared and shifted toward low fields (inset of Fig. 3b).

The temperature dependence of the molar heat capacity of $Co_2B_2O_5$ is shown in Fig. 4. The main feature observed in $C_p(T)$ at $\mu_0 H = 0$ is a λ anomaly at $T_N = 45$ K, which indicates a second order phase transition. In the magnetic field, the λ anomaly is smeared and shifted toward low temperatures so that the singularity at the phase transition at $\mu_0 H = 90$ kOe is identified at 40 K (lower inset of Fig. 4). The specific heat C_p at room temperature does not reach the thermodynamic limit of the lattice contribution to the entropy $3Rz = 224.37$ J/(mol K), where R is the universal gas constant and z is the number of atoms per formula unit. To estimate the anomalous contribution to the

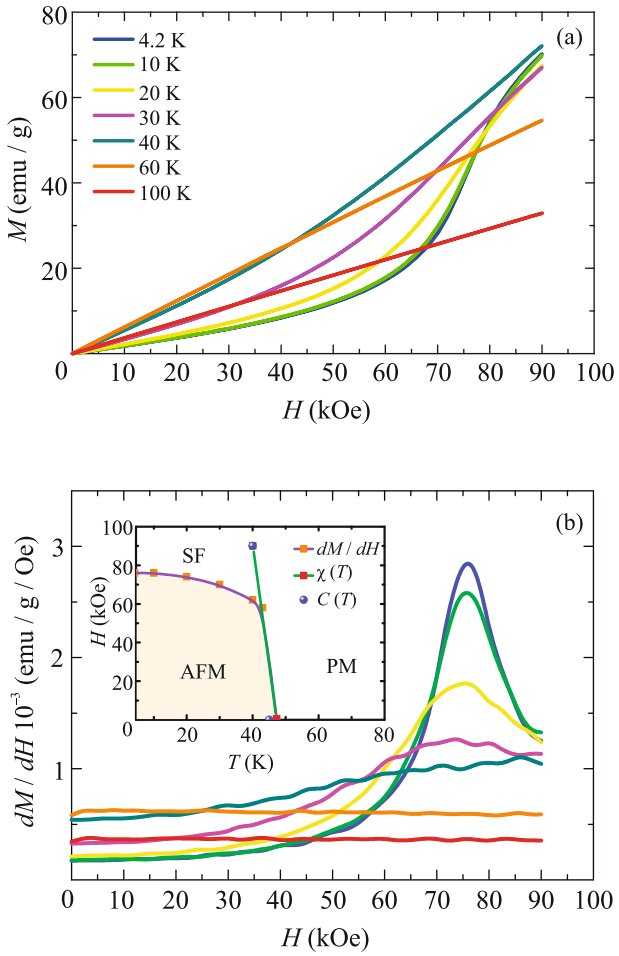

Fig. 3. (Color online) (a) Isotherms of the magnetization of the $Co_2B_2O_5$ single crystal measured in the range of 4.2–100 K. (b) Magnetic-field dependence of the derivative $\partial M/\partial H$. The inset shows the phase diagram of $Co_2B_2O_5$, where AFM, SF, and PM are the antiferromagnetic, spin-flop, and paramagnetic phases, respectively, and the boundaries of the phases are determined from data on the magnetic susceptibility $\chi(T)$, derivative $\partial M/\partial H(H)$, and heat capacity $C(T)$.

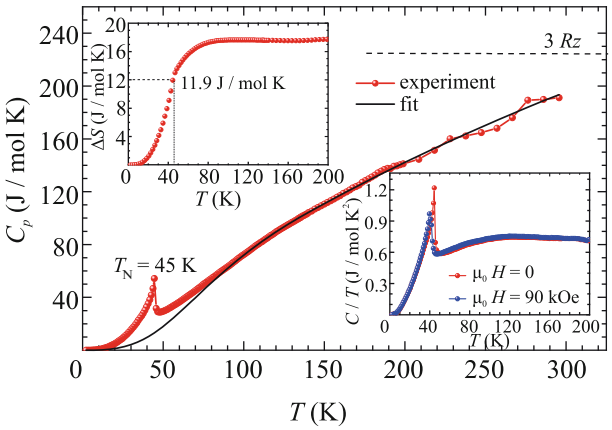

Fig. 4. (Color online) (Circles) Temperature dependence of the molar heat capacity of $Co_2B_2O_5$ measured in zero magnetic field. The solid line is the phonon contribution calculated in the Debye–Einstein approximation. The top inset shows the entropy as a function of the temperature. The entropy $\Delta S_m(T_{N1})$ released at the magnetic transition is marked by the dashed line. The bottom inset shows the shift of the magnetic anomaly in the external magnetic field.

heat capacity, the phonon contribution C_{latt} in temperature ranges far from the anomaly region was processed in the Debye–Einstein approximation. The Debye temperature Θ_D = (428 ± 20) K is in good agreement with values found for other related borates: 493 K (Co_3BO_5 [29]), 356 K ($Co_{1.67}Nb_{0.33}BO_4$ [30]), 299 K (Mn_2BO_4 [9]), and 360 K (V_2BO_4 [10]).

DISCUSSION

The energies of the exchange interactions $|J| = 1.85 \times 10^{-16}$ erg/ion and magnetocrystalline anisotropy $D = 2.15 \times 10^{-17}$ erg/ion for the $Mn_2B_2O_5$ pyroborate were estimated in [22]. The respective estimates for $Co_2B_2O_5$ get values of $|J| = 8.28 \times 10^{-16}$ erg/ion and $D = 4.33 \times 10^{-17}$ erg/ion. Thus, the substitution of the Co^{2+} ion for the Mn^{2+} ion enhances both exchange and anisotropic interactions in agreement with an increase in the magnetic transition temperature in $Co_2B_2O_5$ compared to $Mn_2B_2O_5$. The enhancement of the magnetocrystalline anisotropy in $Co_2B_2O_5$ is not surprising because the single-ion anisotropy of the Co^{2+} ion is much larger than that for the Mn^{2+} ion. The Mn^{2+} ion with the $3d^5$ electronic configuration has zero orbital angular momentum ($S = 5/2$, $L = 0$); as a result, it has small single-ion anisotropy. At the same time, the ground sate of the Co^{2+} ion in the distorted octahedral field can be described, taking into account the spin–orbit coupling, by two Kramers doublets separated by about 100 cm^{-1}. The system at high temperatures is characterized by the effective spin $S = 3/2$ and a small orbital contribution; the corresponding effective moment is about $4.9\mu_B$. At low temperatures, the lowest Kramers doublet is populated. The orbital contribution from the nearest level leads to a large anisotropy of the g-factor if the symmetry of the crystal field is not cubic. Indeed, the analysis of local distortions at Co1 and Co2 sites in $Co_2B_2O_5$ showed that cobalt ions are located in the center of strongly distorted oxygen octahedra [21, 24].

The anomalous entropy is saturated at 100 K and reaches (17.6 ± 0.2) J/(mol K) (upper inset of Fig. 4). The entropy at the magnetic transition point is $\Delta S_m(T_N)$ = (11.9 ± 0.2) J/(mol K). In the mean field theory, the anomalous entropy associated with the long-range magnetic ordering of $n_{Co^{2+}} = 2$ of Co^{2+} magnetic ions with the spin S is given by the expression

$\Delta S_m = n_{Co^{2+}} R \ln(2S+1)$. The experimental total entropy per cobalt ion is $\Delta S_{ion}/R = 0.719$, which is in good agreement with the value $\Delta S_{ion}/R = \ln 2 = 0.692$ associated with the ordering of the Co^{2+} ion whose ground state is the Kramers doublet ($S = 1/2$).

The processing of the experimental data for the magnetic susceptibility disregarding the parameter χ_0 gives the values $\theta = (18 \pm 1)$ K and $C = (6.62 \pm 0.02)$ emu/mol, which correspond to the effective magnetic moment $\mu_{eff} = 5.15\mu_B/Co^{2+}$. Thus, the magnetic parameters obtained in measurements on the single crystal show a small increase compared to values $\theta = 7.7$ K and $\mu_{eff} = 4.96\mu_B/Co^{2+}$ previously determined for the polycrystalline sample in the same way [19]. A reason can be the magnetic anisotropy inherent in these borates that inevitably results in the dependence of the magnetic parameters on the orientation of the external field with respect to the crystal axes [29–31]. Such a behavior is observed, e.g., in cobalt ludwigite Co_3BO_5, where the temperature θ determined for three crystallographic directions differs in both absolute value and sign. The positive sign of the Curie–Weiss temperature found in our and previous studies of $Co_2B_2O_5$ and $Fe_2B_2O_5$ [19, 21] indicates the competition between magnetic interactions of different signs. Examples of antiferromagnetic materials with a positive θ value are dibromides and dichlorides ($Me^{2+}Br_2$ and $Me^{2+}Cl_2$, Me^{2+} = Fe, Co [35]) and ilmenites ($Me^{2+}TiO_3$, Me^{2+} = Fe, Co, Ni [36]), where magnetic ions form hexagonal layers separated by layers of nonmagnetic atoms (halogenides or Ti^{4+}). These compounds undergo an antiferromagnetic transition at low temperatures to structures where magnetic moments in a metal layer are coupled ferromagnetically, whereas coupling between layers is antiferromagnetic.

The magnetic structure of pyroborates can also be considered as the alternating of magnetic layers, which are formed by divalent ions, and nonmagnetic layers consisting of boron atoms (Fig. 1). The magnetic layer is in turn formed by almost hexagonally ordered magnetic ions inside a ribbon. The long-range magnetic order in the crystal is due to antiferromagnetic coupling. This is in agreement with the observation of the λ anomaly in the heat capacity measurements. At the same time, a low but positive θ value reflects the presence of ferromagnetic interactions. A large magnetic moment of about $2.76\mu_B$/f.u. observed at 4.2 K in a field of 90 kOe, which is almost half the expected saturation value $M_s = n_{Co^{2+}} gS\mu_B$, implies that the energy of the external magnetic field becomes comparable with the energy of the magnetic interaction.

The study of the magnetic structure of the $Co_2B_2O_5$ pyroborate should be continued, in particular, using neutron diffraction methods.

CONCLUSIONS

Cobalt pyroborate single crystals have been obtained by spontaneous crystallization from solution–melt. X-ray diffraction measurements showed that the prepared samples are crystallized in the triclinic symmetry $P\bar{1}$. The lattice parameters are close to the previously reported data. The measurements of the static magnetization and heat capacity in the temperature range of 4.2–300 K and in magnetic fields up to 90 kOe have revealed that $Co_2B_2O_5$ undergoes a transition to an antiferromagnetic state at $T_N = 45$ K. The magnetic moment $4.9\mu_B$ is characteristic of a high-spin state of Co^{2+} ions. The sample undergoes the spin-flop transition in the field H_{sf} (4.2 K) = 75 kOe. The analysis of the magnetic parameters has shown that the significant shift of the spin-flop transition in $Co_2B_2O_5$ compared to $Mn_2B_2O_5$ is due to the enhancement of exchange interactions and magnetocrystalline anisotropy. The transition to the antiferromagnetic state is a well-defined phase transition and is manifested in the heat capacity measurements as the λ anomaly at T_N. The Debye temperature determined in the Debye–Einstein approximation is $\Theta_D = (428 \pm 20)$ K.

ACKNOWLEDGMENTS

We are grateful to M.V. Gorev for the discussion of the experimental data on the heat capacity.

FUNDING

This work was supported by the Russian Foundation for Basic Research, project no. 20-02-00559.

REFERENCES

1. H. F. J. Glass, Z. Liu, P. M. Bayley, E. Suard, S. H. Bo, P. G. Khalifah, C. P. Grey, and S. E. Dutton, Chem. Mater. **29**, 3118 (2017).
2. H. Chen, B. B. Xu, Q. S. Ping, B. Z. Wu, X. K. Wu, Q. Q. Zhuang, H. L. Wang, and B. F. Wang, Rare Met. **39**, 1045 (2020).
3. V. Pralong, B. le Roux, S. Malo, A. Guesdon, F. Lainé, J. F. Colin, and C. Martin, J. Solid State Chem. **255**, 167 (2017).
4. V. A. Sarkisyan, I. A. Troyan, I. S. Lyubutin, A. G. Gavrilyuk, and A. F. Kashuba, JETP Lett. **76**, 664 (2002).
5. V. E. Dmitrienko, E. N. Ovchinnikova, S. P. Collins, G. Nisbet, G. Beutier, Y. O. Kvashnin, V. V. Mazurenko, A. I. Lichtenstein, and M. I. Katsnelson, Nat. Phys. **10**, 202 (2014).
6. N. I. Snegirev, I. S. Lyubutin, S. V. Yagupov, A. G. Kulikov, V. V. Artemov, Yu. A. Mogilenets, and M. B. Strugatskii, JETP Lett. **112**, 352 (2020).
7. J. P. Attfield, A. M. T. Bell, L. M. Rodriguez-Martinez, J. M. Greneche, R. J. Cernik, J. F. Clarke, and D. A. Perkins, Nature (London, U.K.) **396**, 655 (1998).

8. R. Norrestam, M. Kritikos, and A. Sjödin, J. Solid State Chem. **114**, 311 (1995).
9. N. V. Kazak, M. S. Platunov, Y. V. Knyazev, N. B. Ivanova, O. A. Bayukov, A. D. Vasiliev, L. N. Bezmaternykh, V. I. Nizhankovskii, S. Yu. Gavrilkin, K. V. Lamonova, and S. G. Ovchinnikov, J. Magn. Magn. Mater. **393**, 316 (2015).
10. E. M. Carnicom, K. Górnicka, T. Klimczuk, and R. J. Cava, J. Solid State Chem. **265**, 319 (2018).
11. P. Bordet and E. Suard, Phys. Rev. B **79**, 144408 (2009).
12. J. Bartolomé, A. Arauzo, N. V. Kazak, N. B. Ivanova, S. G. Ovchinnikov, Yu. V. Knyazev, and I. S. Lyubutin, Phys. Rev. B **83**, 144426 (2011).
13. M. S. Platunov, S. G. Ovchinnikov, N. V. Kazak, N. B. Ivanova, V. N. Zabluda, E. Weschke, E. Schierle, and K. V. Lamonova, JETP Lett. **96**, 650 (2012).
14. C. W. Galdino, D. C. Freitas, C. P. C. Medrano, R. Tartaglia, D. Rigitano, J. F. Oliveira, A. A. Mendonça, L. Ghivelder, M. A. Continentino, D. R. Sanchez, and E. Granado, Phys. Rev. B **100**, 165138 (2019).
15. A. K. Zvezdin, S. S. Krotov, A. M. Kadomtseva, G. P. Vorob'ev, Yu. F. Popov, A. P. Pyatakov, L. N. Bezmaternykh, and E. N. Popova, JETP Lett. **81**, 272 (2005).
16. C. Ritter, A. Vorotynov, A. Pankrats, G. Petrakovskii, V. Temerov, I. Gudim, and R. Szymczak, J. Phys.: Condens. Matter **20**, 365209 (2008).
17. V. Yu. Ivanov, A. M. Kuzmenko, and A. A. Mukhin, JETP Lett. **105**, 435 (2017).
18. J. C. Fernandes, F. S. Sarrat, R. B. Guimar aes, R. S. Freitas, M. A. Continentino, A. C. Doriguetto, Y. P. Mascarenhas, J. Ellena, E. E. Castellano, J.-L. Tholence, J. Dumas, and L. Ghivelder, Phys. Rev. B **67**, 104413 (2003).
19. T. Kawano, H. Morito, and H. Yamane, Solid State Sci. **12**, 1419 (2010).
20. S. C. Neumair and H. Huppertz, Z. Naturforsch., B **64**, 491 (2009).
21. T. Kawano, H. Morito, T. Yamada, T. Onuma, Sh. F. Chichibu, and H. Yamane, J. Solid State Chem. **182**, 2004 (2009).
22. F. S. Sarrat, R. B. Guimarés, M. A. Continentino, J. C. Fernandes, A. C. Doriguetto, and J. Ellena, Phys. Rev. B **71**, 224413 (2005).
23. S. V. Berger, Acta Chem. Scand. **4**, 1054 (1950).
24. J. L. C. Rowsell, N. J. Taylor, and L. F. Nazar, J. Solid State Chem. **174**, 189 (2003).
25. A. Utzolino and K. Bluhm, Z. Naturforsch., B **51**, 912 (1996).
26. S. Busche and K. Bluhm, Z. Naturforsch. B **50**, 1445 (1995).
27. R. D. Shannon, Acta Crystallogr., A **32**, 751 (1976).
28. L. A. Solovyov, J. Appl. Crystallogr. **37**, 743 (2004).
29. N. V. Kazak, M. S. Platunov, Yu. V. Knyazev, M. S. Molokeev, M. V. Gorev, S. G. Ovchinnikov, Z. V. Pchelkina, V. V. Gapontsev, S. V. Streltsov, J. Bartolomé, A. Arauzo, V. V. Yumashev, S. Yu. Gavrilkin, F. Wilhelm, and A. Rogalev, Phys. Rev. B **103**, 094445 (2021).
30. N. V. Kazak, N. A. Belskaya, E. M. Moshkina, L. N. Bezmaternykh, A. D. Vasiliev, J. Bartolome, A. Arauzo, D. A. Velikanov, S. Yu. Gavrilkin, M. V. Gorev, G. S. Patrin, and S. G. Ovchinnikov, J. Magn. Magn. Mater. **534**, 168056 (2021).
31. N. V. Kazak, M. S. Platunov, N. B. Ivanova, Yu. V. Knyazev, L. N. Bezmaternykh, E. V. Eremin, A. D. Vasil'ev, O. A. Bayukov, S. G. Ovchinnikov, D. A. Velikanov, and Ya. V. Zubavichus, J. Exp. Theor. Phys. **117**, 94 (2013).
32. B. Dojer, A. Pevec, F. Belaj, Z. Jagličić, M. Kristl, and M. Drofenik, J. Mol. Struct. **1076**, 713 (2014).
33. H. -J. Koo, R. K. Kreme, and M.-H. Whangbo, Inorg. Chem. **59**, 18319 (2020).
34. Y. M. Oey and R. Cava, Mater. Res. Bull. **122**, 110667 (2020).
35. M. A. McGuire, Crystals **7**, 121 (2017).
36. H. Watanabe, H. Yamauchi, and H. Takei, J. Magn. Magn. Mater. **15–18,** 549 (1980).

Translated by R. Tyapaev